ACS APPLIED MATERIALS & INTERFACES

Research Article

www.acsami.org

Three-Dimensional Nanoporous Cellulose Gels as a Flexible Reinforcement Matrix for Polymer Nanocomposites

Zhuqun Shi,[†,‡] Junchao Huang,[†,‡] Chuanjun Liu,[†] Beibei Ding,[†] Shigenori Kuga,[§] Jie Cai,*[,†] and Lina Zhang[†]

[†]College of Chemistry & Molecular Sciences, Wuhan University, Wuhan 430072, People's Republic of China

[§]Graduate School of Agricultural and Life Sciences, The University of Tokyo, Tokyo, Japan

Supporting Information

ABSTRACT: With the world's focus on utilization of sustainable natural resources, the conversion of wood and plant fibers into cellulose nanowhiskers/nanofibers is essential for application of cellulose in polymer nanocomposites. Here, we present a novel fabrication method of polymer nanocomposites by in-situ polymerization of monomers in three-dimensionally nanoporous cellulose gels (NCG) prepared from aqueous alkali hydroxide/urea solution. The NCG have interconnected nanofibrillar cellulose network structure, resulting in high mechanical strength and size stability. Polymerization of the monomer gave P(MMA/BMA)/NCG, P(MMA/BA)/NCG nanocomposites with a volume fraction of NCG ranging from 15% to 78%. SEM, TEM, and XRD analyses show that the NCG are finely distributed and preserved well in the nanocomposites after polymerization. DMA analysis demonstrates a significant improvement in tensile storage modulus E' above the glass transition temperature; for instance, at 95 °C, E' is increased by over 4 orders of magnitude from 0.03 MPa of the P(MMA/BMA) up to 350 MPa of nanocomposites containing 15% v/v NCG. This reinforcement effect can be explained by the percolation model. The nanocomposites also show remarkable improvement in solvent resistance (swelling ratio of 1.3−2.2 in chloroform, acetone, and toluene), thermal stability (do not melt or decompose up to 300 °C), and low coefficients of thermal expansion (in-plane CTE of 15 ppm·K^{-1}). These nanocomposites will have great promising applications in flexible display, packing, biomedical implants, and many others.

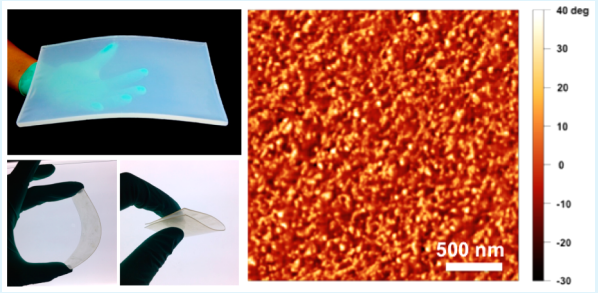

KEYWORDS: *nanoporous cellulose gels, polymer nanocomposites, solvent resistance, mechanical properties, thermal expansion*

INTRODUCTION

Polymer nanocomposites composed of organic polymers and rigid nanocomponents such as carbon nanotubes,[1−4] graphene,[5−9] delaminated clay,[10−12] cellulose nanowhiskers/nanofibrils,[13−20] and bacterial cellulose[21−23] in the form of one-, two-, or three-dimensional architectures provide rich possibilities leading to various advanced materials. Among these, cellulose nanowhiskers/nanofibrils and bacterial cellulose attract special attention due to their sustainability, low-cost availability, and remarkable physical properties, such as a low density of 1.6 g/cm^3, high elastic modulus of 100−200 GPa, and low thermal expansivity of 0.1 ppm/K.[18−20,24,25] Also, the hydroxyl group of cellulose provides many possibilities for chemical modification of nanofiber surfaces useful in nanocomposite preparation.

The main challenge in fabricating cellulose-based nanocomposites is preparation of well-individualized cellulose nanowhiskers/nanofibrils and their dispersion in the polymer matrix with a broad range of composition controls. Several attempts to prepare cellulose-based polymer nanocomposites have been reported. They include surface modification by covalent groups or surfactants adsorption to disperse cellulose in organic solvents, which can be dry cast to form nanocomposites.[26−30] Also, direct dispersion of cellulose nanowhiskers/nanofibrils was attempted from aqueous suspension by a solvent-exchange sol−gel process, freeze drying, or supercritical CO_2 drying techniques.[16,17,21−23,31−36]

While these works used cellulose nanowhiskers/nanofibrils maintaining the native crystallinity, cellulose can be shaped as regenerated hydrogel via dissolution and coagulation. The recently found aqueous alkali hydroxide−urea solvent is particularly suited for gel preparation, and the resulting cellulose aerogels have been shown to give remarkable mechanical strength, high light transmittance, and high porosity of nanometer orders.[37−39] It also has been shown to be useful to give mechanically tough, foldable, and transparent cellulose bioplastics.[40]

Owing to the ease of preparation and processing, we developed a strategy for the cellulose−polymer hybridization via in-situ polymerization of synthetic polymers in three-

Received: July 11, 2015
Accepted: September 23, 2015
Published: September 23, 2015

DOI: 10.1021/acsami.5b06232
ACS Appl. Mater. Interfaces 2015, 7, 22990−22998

dimensionally nanoporous cellulose gels (NCG). The polymers chosen were poly(methyl methacrylate/butyl methacrylate) (P(MMA/BMA)) and poly(methyl methacrylate/butyl acrylate) (P(MMA/BA)). We obtained the nanocomposites with finely distributed NCG in polymer matrix, and a maximum NCG loading of 78% v/v was achieved. Different from the cellulose nanowhiskers/nanofibrils, the NCG fabricated by our approach is a monolith of an interconnected nanofibrillar cellulose network structure, resulting from the entanglement of cellulose chains and interchain hydrogen-bonding interactions.[41] Therefore, we expect to observe superior mechanical reinforcement, solvent resistance, and thermal properties of the NCG-based polymer nanocomposites.

EXPERIMENTAL SECTION

Materials. All materials and reagents were used as received. Organic solvents, lithium hydroxide hydrate, urea, sodium sulfuric, sulfuric acid, methyl methacrylate (MMA), butyl methacrylate (BMA), butyl acrylate (BA), and benzoyl peroxide were purchased from Shanghai Chemical Reagent Co. Ltd., China. Cellulose (cotton linter pulp) was provided by Hubei Chemical Fiber Co. Ltd. (Xiangfan, China). The weight-average molecular weight (M_w) was determined by dynamic laser scattering (DLS, ALV/CGS-8F, ALV, Germany) in aqueous 4.6 wt % LiOH/15 wt % urea solution to be 9.2×10^4.[42]

Fabrication of NCG by the Sol−Gel Process. Cellulose was dissolved in an aqueous 4.6 wt % LiOH/15 wt % urea precooled to −12 °C to form 5 wt % transparent cellulose solution within 3 min according to our previous method.[43] The cellulose solution was subjected to centrifugation to remove air bubbles and subsequently spread on glass molds and coagulated by ethanol to form gels, followed by thorough washing with deionized water to give NCG hydrogels with different thickness (1, 3, 5, and 7 mm).

Fabrication of Dried NCG Film. The NCG hydrogel with 0.9 mm thickness was fixed on a plastic plate at ambient temperature to evaporate the water and dry the resulting film, which had a thickness of ca. 90 μm.

Fabrication of NCG Aerogel. The hydrogel was solvent exchanged to ethanol and then dried from supercritical CO_2 to obtain aerogel, which had a thickness of ca. 0.9 mm. Supercritical CO_2 drying was performed by a Hitachi HCP-2 by exchanging ethanol to liquid CO_2 at 5.3 MPa at 4 °C for 6 h, then at 10 MPa for 0.5 h at 40 °C, and finally by slow release of CO_2 at 40 °C.

Fabrication of P(MMA/BMA)/NCG Nanocomposites by in-Situ Polymerization. The four thickness-series hydrogels were compressed under 0.2 MPa at 60 °C to ca. 0.9 mm to achieve NCG hydrogels with different water content, i.e., various porosities. These NCG hydrogels were subjected to solvent exchange with acetone and then placed into monomer solutions with various ratios of methyl methacrylate (MMA) and butyl methacrylate (BMA) containing 5% (w/v) benzoyl peroxide as initiator at ambient temperature for 12 h. The gels were subsequently removed from the monomer solutions, sealed into glass mold to prevent solution evaporation, and heated at 47 °C for 12 h to polymerize and then 90 °C for 3 h to remove the residual monomer. All references to P(MMA/BMA) refer to P(MMA/BMA) polymerized from a monomer ratio of 3:7, unless specified otherwise.

Fabrication of P(MMA/BA)/NCG Nanocomposites by in-Situ Polymerization. The NCG hydrogels with different porosities were subjected to solvent exchange with acetone and then placed into monomer solutions with various ratios of methyl methacrylate (MMA) and butyl acrylate (BA) containing 5% (w/v) benzoyl peroxide as initiator at ambient temperature for 12 h. The gels were subsequently removed from the monomer solutions, sealed into a glass mold to prevent solution evaporation, and heated at 47 °C for 12 h to polymerize and then 90 °C for 3 h to remove the residual monomer. All references to P(MMA/BA) refer to P(MMA/BA) polymerized from a monomer ratio of 3:7, unless specified otherwise.

Determination of Volume Fraction of NCG in Nanocomposites. The volume fraction of NCG of the nanocomposites was determined gravimetrically as an average of at least 3 independently prepared samples. Before fabrication of nanocomposites, the water content of the NCG hydrogel was calculated from swollen and dried state. On the other hand, the imbibed water in weighted hydrogels was solvent exchanged to acetone and then to monomers containing initiator. After in-situ polymerization, the nanocomposites were weighted. The densities of cellulose, PMMA, PBMA, and PBA are 1.62, 1.18, 1.07, and 1.08 g/cm^3, respectively. Hence, the densities of P(MMA/BMA) and P(MMA/PBA) are both about 1.11 g/cm^3.

Characterization. *Wide Angle X-ray Diffraction (WAXD).* Wide angle X-ray diffraction (WAXD) measurement was carried out on a WAXD diffractometer (D8-Advance, Bruker, USA). The X-ray used was Ni-filtered Cu Kα radiation with a wavelength of 1.542 Å. The voltage was set at 40 kV, and the current was set at 40 mA. The samples were mounted on a solid circular holder, and the proportional counter detector was set to collect data at a rate of $2\theta = 2°$ min^{-1} over the 2θ range from 8° to 40°.

Scanning Electron Micrograph (SEM). For microscopic examination, the imbibed water of hydrogels was solvent exchanged to acetone, toluene, or hexane and then subjected to supercritical CO_2 drying to give aerogels. Supercritical CO_2 drying was performed by a Hitachi HCP-2 by exchanging ethanol to liquid CO_2 at 5.3 MPa at 4 °C for 6 h, then at 10 MPa for 0.5 h at 40 °C, and finally by slow release of CO_2 at 40 °C. Samples used for scanning electron microscopy (SEM) analysis were coated and examined by a Hitachi S-4000 microscope.

Atomic Force Microscopy (AFM). The cross-section of the nanocomposites was examined by AFM (MultiMode 8, Bruke, USA) to acquire topography and phase images in tapping mode. The samples were embedded into epoxy resin and microtomed to obtain smooth surfaces by a Leica Ultracut-E using a diamond knife.

Transmission Electron Micrograph (TEM). For transmission microscopy (TEM) the nanocomposites were immersed in a 7:3 mixture of hydroxyethyl methacrylate and butyl methacrylate containing 1.4% (w/v) benzoyl peroxide as initiator. After polymerization by curing at 52 °C overnight, the embedded specimen was sectioned by a Leica Ultracut-E using a diamond knife. The sections of approximately 100 nm thick (gold color) were mounted on a grid with carbon support and then disembedded by removing the resin by acetone. The section was then examined by a JEOL-1010 without staining (defocus contrast).

Optical Transmittance Testing. Light transmission of the nanocomposites and neat polymers was performed on a UV-160A spectrophotometer (Shimadzu, Japan) using a quartz cuvette with an optical path of 1 cm at wavelengths ranging from 400 to 800 nm. A sheet of sample was set on the cell for each measurement. The thickness of the sheets was about 0.9 mm.

Water Uptake. Water uptake was evaluated by immersing samples in deionized water at room temperature for 24 h. The sample was oven dried at 60 °C for 24 h, and then the water uptake was determined by measuring the weight of the samples pre- and postswelling

$$(\text{mass of wet sample} - \text{mass of dry sample})/\text{mass of dry sample} \times 100\%$$

Swelling Ratio. Swollen ratio was evaluated by immersing samples in organic solvents at room temperature for 24 h. The sample was oven dried at 60 °C for 24 h, and then the swelling ratio was determined by measuring the volume of the samples pre- and postswelling

$$(\text{volume of swollen sample} - \text{volume of dry sample})/\text{volume of dry sample} \times 100\%$$

Contact Angle (CA) Testing. Contact angles of the nanocomposites were evaluated on a Data Physics Instrument (Drop shape analysis system DSA-100/10, Krüss) in dynamic mode. One drop of water (3

DOI: 10.1021/acsami.5b06232
ACS Appl. Mater. Interfaces 2015, 7, 22990−22998

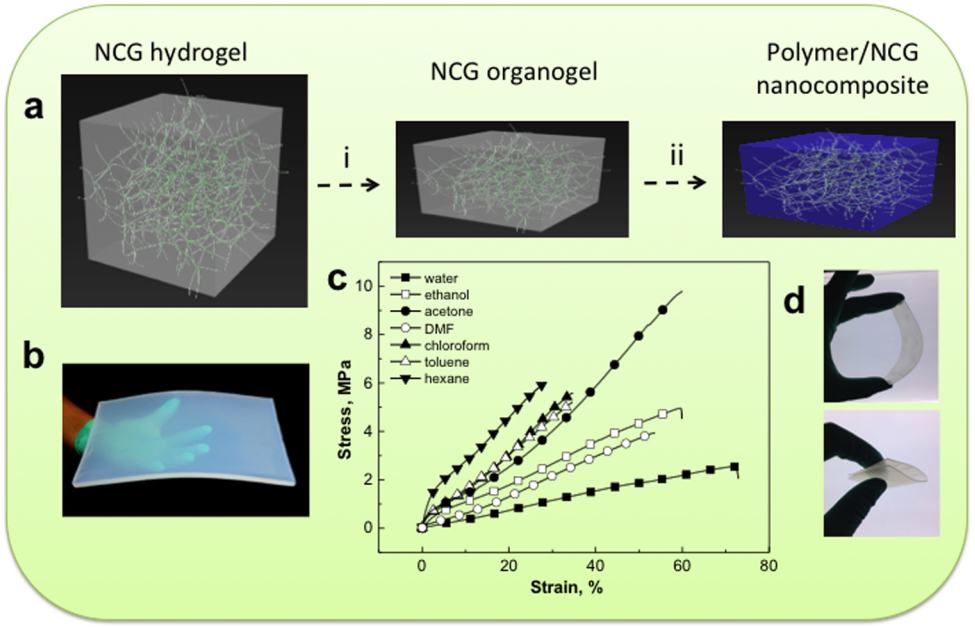

Figure 1. (a) Preparation of polymer/NCG nanocomposites: (i) NCG hydrogel with interconnected nanofibrillar network is compressed and solvent exchange with acetone to form NCG organogel; (ii) polymer polymerization is achieved by placing NCG organogel into monomer solutions with various ratios of methyl methacrylate (MMA), butyl methacrylate (BMA), and butyl acrylate (BA) containing benzoyl peroxide as initiator and then in-situ polymerization giving polymer/NCG nanocomposites. (b) Photograph of the NCG hydrogel. (c) Stress–strain curves of the NCG hydrogel and organogels prepared by solvent exchange from the hydrogels with 92 wt % water content. (d) Macroscopic views of the P(MMA/BMA)/NCG (top) and P(MMA/BA)/NCG (bottom) nanocomposites.

μL) was dropped on their surface with an automatic piston syringe and photographed.

Thermogravimetry Analysis (TGA). TGA for the NCG, polymers, and nanocomposites were performed on a TG instrument (Perkin-Emer Co., USA) in an atmosphere of nitrogen at a heating rate of 10 °C/min from 30 to 600 °C.

Dynamic Mechanical Analysis (DMA). DMA temperature sweeps under oscillatory stress were performed on the nanocomposites, neat polymers, and NCG film using a DMA Q800 (TA Instrument, USA) in tensile mode at a heating rate of 5 °C/min in the temperature range from −100 to 200 °C with a frequency of 1 Hz.

Tensile Test. Stress–strain experiments were performed at ambient temperature on a universal tensile tester (CMT 6503, SANS Test machine Co. Ltd., China) with a tension speed of 5 mm/min. The modulus was calculated from the initial linear region of the stress–strain curves.

Coefficient of Thermal Expansion (CTE). The CTEs were measured by a thermomechanical analyzer (TMA Q400, TA, USA). The measurements were carried out in plane and thickness directions at a heating rate of 5 °C/min under nitrogen atmosphere. The CTE values were determined at 20–200 °C in the second run.

RESULTS AND DISCUSSION

Figure 1 shows the preparation of the NCG/polymer nanocomposites. The NCG hydrogel obtained from aqueous alkali–urea solvent is a nearly transparent and self-standing material having a water content of 92% and porosity of 95% (Figure 1b). The hydrogel was compressed and then solvent exchanged with acetone to form NCG organogel. Subsequently, the NCG organogel was placed into monomer solutions with various ratios of methyl methacrylate (MMA), butyl methacrylate (BMA), and butyl acrylate (BA) containing benzoyl peroxide as initiator. After the removal of excess liquid from the surface, the gel sheet was subjected to in-situ polymerization of acrylate monomers in the NCG matrix, giving polymer/NCG nanocomposites.

An outstanding feature of the NCG superior to cellulose nanowhiskers/nanofibrils gels is its high mechanical strength and size stability, resulting from strong interchain hydrogen-bonding interactions and entanglement of cellulose chains.[41] This feature allows keeping the shape and size of the NCG after easy solvent-exchange processes, which can be done by mere dipping of NCG piece in miscible liquids step by step, i.e., from water to ethanol or acetone and then to toluene or hexane. These NCG hydrogels and organogels are robust, and 2 g gels could support 200 g in weight without any deformation (see Figure S1 in the Supporting Information). For microscopic examination, the imbibed water of hydrogels was solvent exchanged to acetone, toluene, or hexane and then subjected to supercritical CO_2 drying to give aerogels. Scanning electron microscopy (SEM) revealed a homogeneous nanoporous network of interconnected cellulose nanofibrils in the NCG and preserved well throughout solvent-exchange processes (see Figure S2 in the Supporting Information). Remarkably, the NCG organogels are tougher than hydrogel; for instance, the tensile modulus and strength were determined as 3.5 and 2.6 MPa for hydrogel and 104 and 6.0 MPa for hexane organogel (Figure 1c and Table 1). Such high mechanical integrity is not obtained on cellulose nanowhiskers/nanofibril gels.

The NCG content of the nanocomposites can be controlled by changing the water content of starting NCG hydrogels by squeezing out water under slow compression. The maximum possible compression was to 1/10 of the original thickness, i.e., to more than 90% solid (see Figure S3 in the Supporting Information). Polymerization of the monomer solutions gave P(MMA/BMA)/NCG, P(MMA/BA)/NCG nanocomposites with the volume fraction of NCG ranging from 15% to 78% (see Figure S4 in the Supporting Information). The tough P(MMA/BMA)/NCG and foldable P(MMA/BA)/NCG (Figure 1d) nanocomposites, which are approximately 1 mm thick,

DOI: 10.1021/acsami.5b06232
ACS Appl. Mater. Interfaces 2015, 7, 22990–22998

Table 1. Mechanical Properties of NCG Hydrogels and Organogels Prepared by Solvent Exchange from the Hydrogels with 92 wt % Water Content

solvents	σ_b (MPa)	ε (%)	E (MPa)	polarity index
water	2.6	72	3.5	10.2
N,*N*-dimethylformamide	3.9	53	6.3	6.4
acetone	9.7	60	54.6	5.4
chloroform	5.6	35	50.3	4.4
ethanol	5.0	60	23.6	4.3
toluene	5.2	34	67.5	2.4
hexane	6.0	28	104	0.06

were fairly transparent, thus demonstrating their homogeneous dispersion of NCG in the nanocomposites.

Microscopic morphology and structure of the nanocomposites were examined by AFM by tapping mode. The topography images and phase contrast images on the inner part of the P(MMA/BMA)/NCG (Figure 2a and 2b) and P(MMA/BA)/NCG (see Figure S5 in the Supporting Information) nanocomposites revealed uniform morphology with emerging of the NCG in P(MMA/BMA) and P(MMA/BA) matrix. Moreover, the images of the ultramicrotomed samples reveal a homogeneous distribution of light nanofibrillar network structure, similar to that of neat NCG by SEM observation (Figure 2c), against a darker background. Furthermore, the interconnected nanofibrillar cellulose network was also observed by transmission electron microscopy (TEM) of an ultrathin section of the P(MMA/BMA)/NCG nanocomposite (Figure 2d), from which the resin was removed by solvent on the specimen grid. Overall, the images support that the interconnected nanofibrillar cellulose network structure of the NCG is preserved well and finely distributed in the nanocomposites after in-situ polymerization.

The X-ray diffraction (XRD) patterns are nearly systematic superposition of those of NCG and polymers (see Figure S6 in the Supporting Information), indicating no interference between structure formation of the components. These results, together with the microscopic observation, give a consistent picture, i.e., the nanocomposites have macroscopically homogeneous but microscopically separated-phase structure to give certain superposition of properties of the two components.

The thermomechanical properties of the nanocomposites were established by dynamic mechanical analysis (DMA), in which the glass transition temperature (T_g) is sometimes referred to the α-relaxation process of chain segments. Figure 3a shows temperature sweep of dynamic modulus at 1 Hz of the P(MMA/BMA)/NCG nanocomposites with different volume fraction of NCG. As a consequence of the already rather high stiffness of the glassy P(MMA/BMA) matrix, the P(MMA/BMA)/NCG nanocomposites exhibit a modest increase of tensile storage moduli (E') below T_g. However, above T_g, the nanocomposite displays a significant mechanical reinforcement over the P(MMA/BMA). For example, at 95 °C, E' is increased by over 4 orders of magnitude from 0.03 MPa for the P(MMA/BMA) to 350 MPa for the P(MMA/BMA)/NCG nanocomposites containing 15% v/v NCG. From the maximum in loss tangent (tan δ) (Figure 3b), the P(MMA/BMA) has a T_g of around 67 °C. The introduction of NCG into P(MMA/BMA) matrix slightly lowered T_g to 54 °C, which is independent of the NCG content. The FT-IR spectra of nanocomposites are a superposition of those of cellulose and polymers (see Figure S7 in the Supporting Information), while the peak from O−H stretching of cellulose shifts from 3337 to 3373 cm^{-1}, suggesting the presence of hydrogen-bonding interaction between cellulose and polymer matrix in the nanocomposites. The intensity of the tan δ peak decreased more than proportionally to the NCG content, which can be understood as the attractive polymer−cellulose matrix interactions leading to the pronounced reduction in chain relaxation.[16] The P(MMA/BA)/NCG nanocomposites gave

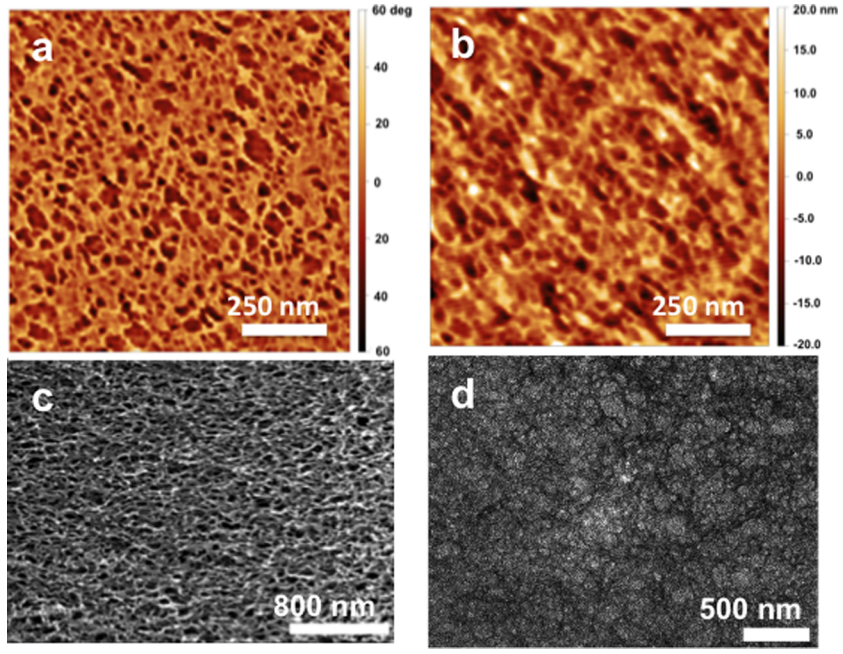

Figure 2. AFM topography image (a) and phase contrast image (b) of the inner part of the P(MMA/BMA)/NCG nanocomposites containing 15% v/v NCG. (c) SEM images of the inner part of the NCG aerogel. (d) TEM image of a disembedded ultrathin section of the NCG in P(MMA/BMA)/NCG nanocomposite.

DOI: 10.1021/acsami.5b06232
ACS Appl. Mater. Interfaces 2015, 7, 22990−22998

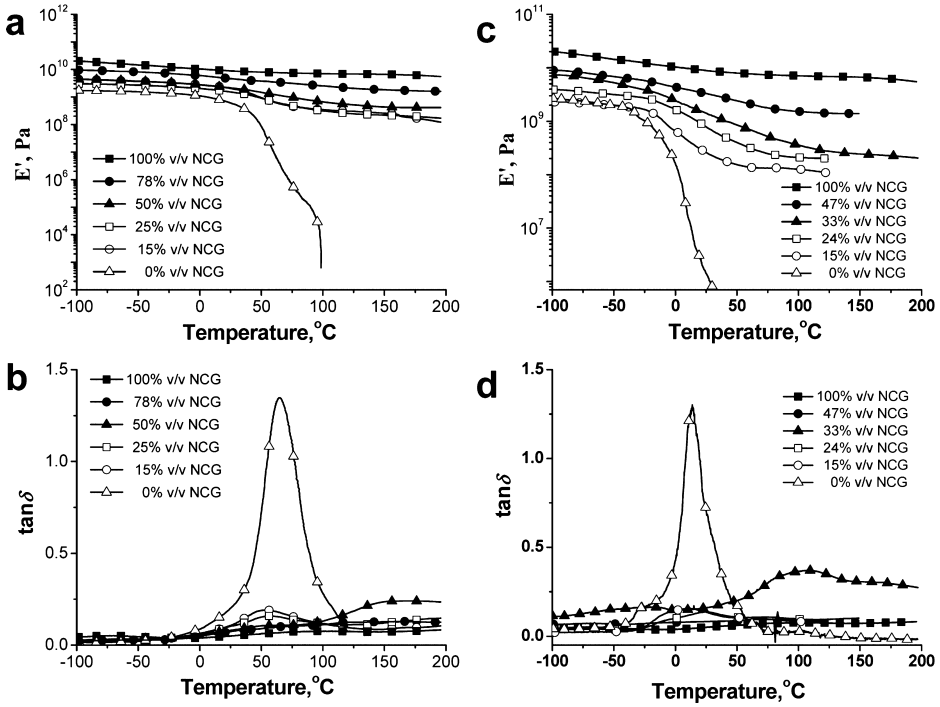

Figure 3. DMA temperature sweeps for P(MMA/BMA)/NCG) and P(MMA/BA)/NCG nanocomposites. Storage modulus E' (a) and loss tangent tan δ (b) of P(MMA/BMA)/NCG nanocomposites as a volume function of NCG and temperature. E' (c) and tan δ (d) of P(MMA/BA)/NGC nanocomposites as a function of volume fraction of NCG and temperature.

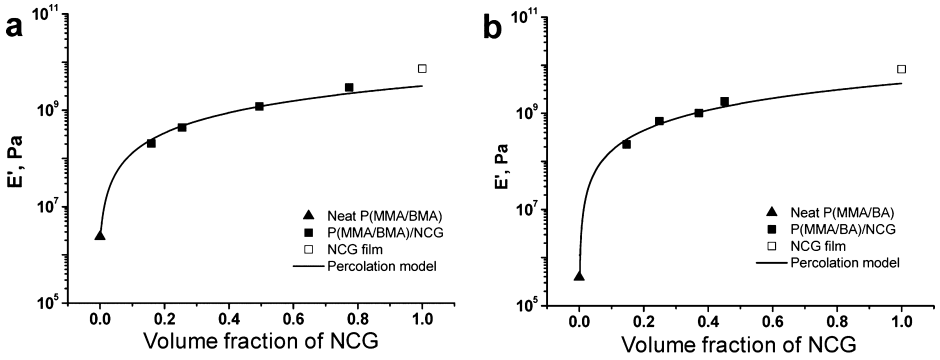

Figure 4. E' above T_g of P(MMA/BMA)/NCG (a) and P(MMA/BA)/NCG (b) nanocomposites plotted against volume fraction of NCG. Curves show prediction by the percolation model. Moduli of the NCG film are also shown.

similar results (Figure 3c and 3d). Moreover, this NCG approach allows for the fabrication of nanocomposites with tunable T_g ranging from −29 to 90 °C by adjusting monomer ratio and improved mechanical properties (see Figures S8 and S9 in the Supporting Information).

Figure 4a and 4b shows the NCG-content dependence of modulus of nanocomposites above T_g. The presence of NCG of only 15% v/v enhanced the modulus by 2 to 3 orders of magnitude from those of neat polymers. Dependence of elastic modulus on cellulose content has been studied numerous times for cellulose-based nanocomposites, with interpretation by the percolation model giving E' of the nanocomposites as[13,15,16,31,44]

$$E' = \frac{(1 - 2\psi + \psi X_r)E_s'E_r' + (1 - X_r)\psi E_e'^2}{(1 - X_r)E_r' + (X_r - \psi)E_s'} \quad (1)$$

with

$$\psi = X_r\left(\frac{X_r - X_c}{1 - X_c}\right)^{0.4} \quad (2)$$

and

$$X_c = \frac{0.7}{f} \quad (3)$$

where $E_s' = E'$ of neat polymer, $E_r' = E'$ of percolating cellulosic network, X_r = volume fraction of nanowhiskers/nanofibrils, X_c = volume fraction of nanowhiskers/nanofibrils at percolation threshold, ψ = volume fraction of nanowhiskers/nanofibrils contributing to percolation ("effective skeleton"), and f = aspect ratio of nanowhiskers/nanofibrils.

Since the NCG is intrinsically percolated as long as it is a "gel", X_c must be set zero, making eq 3 irrelevant. Equation 2 is based on the assumption that elastic modulus is proportional to percolation probability, i.e., the fraction of fibrous elements belonging to spanning clusters, or "effective skeleton".[45,46] Here

DOI: 10.1021/acsami.5b06232
ACS Appl. Mater. Interfaces 2015, 7, 22990−22998

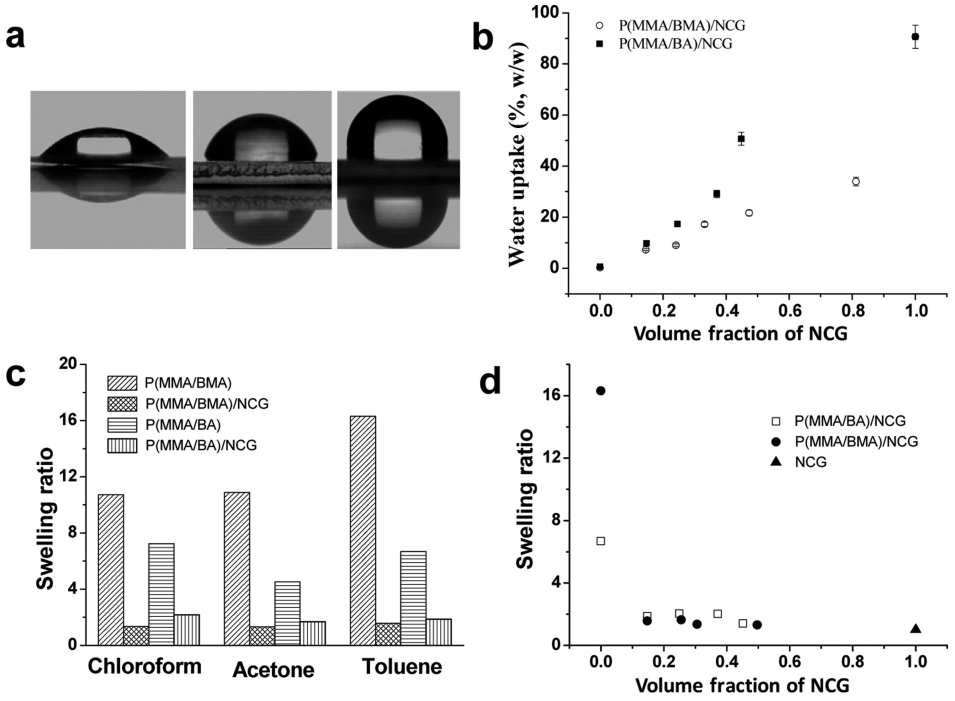

Figure 5. (a) Water contact angle photographs of NCG (left), P(MMA/BMA)/NCG (middle), and P(MMA/BA)/NCG (right) nanocomposites containing 15% v/v NCG. (b) Water uptake of the nanocomposites as a function of volume fraction of NCG for 48 h immersion. (c) Swelling ratio of P(MMA/BMA), P(MMA/BA), P(MMA/BMA)/NCG, and P(MMA/BA)/NCG nanocomposites containing 15% v/v NCG in chloroform, acetone, and toluene at ambient temperature for 2 weeks. (d) Swelling ratio of the nanocomposites as a function of volume fraction of NCG in toluene for 2 weeks.

again, use of this formula to gel is questionable because all elements of a gel belong to an infinite network. Nevertheless, the experimentally determined E' values of the nanocomposites with various volume fractions of NCG agree well with the percolation model by using experimental values for X_p, E_s' (2.4 MPa for P(MMA/BMA) and 0.4 MPa for P(MMA/BA)) and fitting values from the experimental data for E_r' (3.2 GPa for P(MMA/BMA)/NCG nanocomposites and 4.2 GPa for P(MMA/BA)/NCG nanocomposites), supporting the conclusion that the three-dimensional NCG indeed forms a percolating network and is preserved well in the nanocompositses. Notably, there are obvious differences between the E_r' values for cellulose nanofibrils (10 GPa),[13] nanowhiskers (ranging from 0.25 to 80 GPa),[15−17,31,47−53] and NCG (3.2 and 4.2 GPa in this work), suggesting that nanofiller−nanofiller interactions in polymer nanocomposites are strongly dependent on the type of cellulose material, architecture of cellulose, and polarity of polymer matrix. The agreement with calculation is even better than for cellulose nanowhikers/nanofibrils-based nanocomposites to which the percolation model seems to be appropriate. Thus, the scaling law formula of eq 2 may be used as a phenomenological description of the gel-type nanocomposite, while understanding of this behavior awaits further studies.

Practical uses of these nanocomposites may involve contact with water or organic solvents. We therefore examined water contact angle and solvent resistance of the nanocomposites. The water contact angles of the dried NCG, P(MMA/BMA)/NCG, and P(MMA/BA)/NCG (15% v/v NCG content) were 63°, 79°, and 105° (Figure 5a), respectively. Expectably, hybridization with P(MMA/BMA) and P(MMA/BA) made the NCG more hydrophobic. Moreover, the nanocomposites showed remarkably improved water resistance over the NCG. Dried P(MMA/BMA)/NCG and P(MMA/BA)/NCG nanocomposites containing 15% v/v NCG were immersed into deionized water to achieve equilibrium swelling of around 9% w/w) (see Figure S10 in the Supporting Information). Neat P(MMA/BMA) and P(MMA/BA) have water uptake values (both of ∼0.5% w/w) with only minor variations within 26 days. Swelling by deionized water after 48 h immersion was nearly proportional to NCG content of the nanocomposites (Figure 5b), an inevitable feature due to hydrophilicity of cellulose.

Resistance to organic solvents (chloroform, acetone, and toluene) is opposite for water. For example, the neat P(MMA/BMA) was significantly swollen and softened in toluene overnight, but the P(MMA/BMA)/NCG nanocomposites showed better dimensional stability even in toluene for more than 1 month (Figure 5c; see Figure S11 in the Supporting Information). Swelling ratios of neat P(MMA/BMA) are around 10.8 in chloroform and acetone and 16.3 in toluene. The neat P(MMA/BA) also display large swelling ratios between 4.5 and 7.2. In contrast, the P(MMA/BMA) and P(MMA/BA) nanocomposites showed much lower swelling ratios of 1.3−2.2 in those organic solvents. Moreover, the toluene swelling ratio of these nanocomposites is nearly independent of the NCG content (Figure 5d). This feature confirms again that the three-dimensional NCG may contribute such solvent resistance in the nanocomposites, in which barrier effects coming from the interconnected nanofibrillar cellulose network are facilitated through strong interchain hydrogen-bonding interactions and entanglement of cellulose chains.[41] Since these nanocomposites have excellent solvent resistance, especially in organic solvents, they should have broader applicability than neat polymers.

DOI: 10.1021/acsami.5b06232
ACS Appl. Mater. Interfaces 2015, 7, 22990−22998

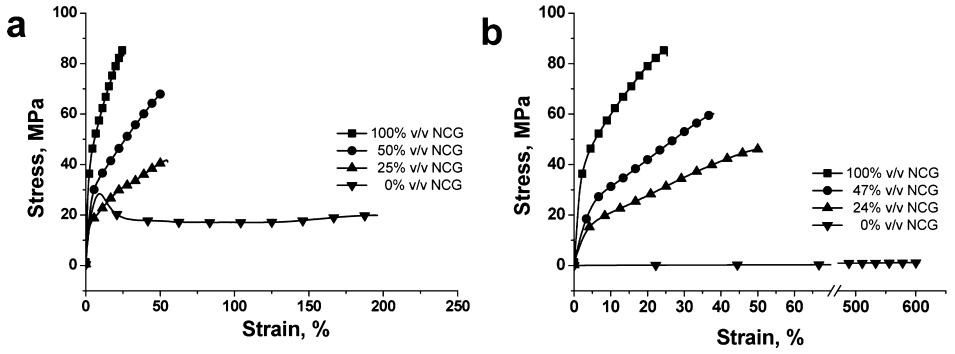

Figure 6. Stress–strain curves of the P(MMA/BMA)/NCG (a) and P(MMA/BA)/NCG nanocomposites (b) with a different volume fraction of NCG.

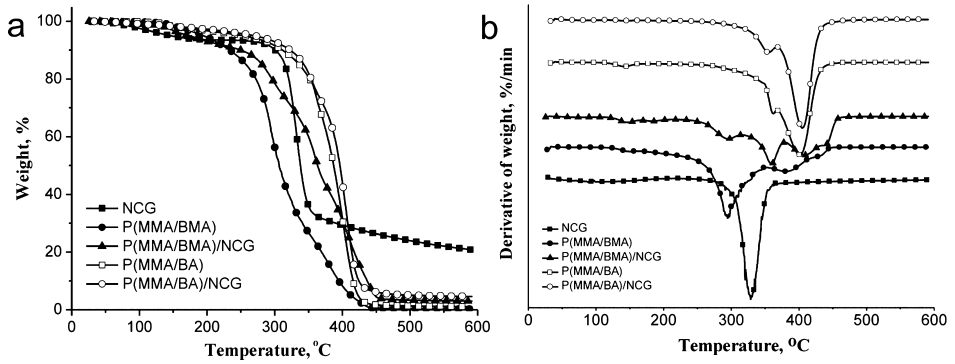

Figure 7. Thermogravimetry (a) and derivative thermogravimetry (b) curves of NCG, P(MMA/BMA), P(MMA/BA), and the nanocomposites containing 15% v/v NCG under nitrogen atmosphere.

To further demonstrate the solvent resistance of the nanocomposites, a weight of 100 g was clung onto a thin copper wire that was prefixed on the downside of a P(MMA/BMA)/NCG nanocomposite sheet (4.5 mm by 50 mm) containing 15% v/v NCG and immersed into toluene. The thickness of the sheets is 0.9 mm. The nanocomposite sheet showed hardly any deformation under a tension force of 24 N/cm^2 in toluene for more than 1 month (see Figure S12 in the Supporting Information).

The stress–strain curves at 25 °C show that the neat P(MMA/BMA) and P(MMA/BA) are in glassy state and rubbery state, respectively (Figure 6). Notably, all P(MMA/BMA)/NCG and P(MMA/BA)/NCG nanocomposites exhibit an elastic nonlinear behavior, independent of the aggregation structure of the polymer matrix. The tensile strength increased from 28 MPa for neat P(MMA/BMA) (stress at yield) to 70 MPa for P(MMA/BMA)/NCG nanocomposites containing 50% v/v NCG (stress at break) and to more than 50 times from 1.0 MPa for neat P(MMA/BA) to 59 MPa for P(MMA/BA)/NCG nanocomposites containing 47% v/v NCG (stress at break), whereas the elongations at break were reduced from 196% to 50% for P(MMA/BMA)/NCG nanocomposites and from 606% to 37% for P(MMA/BA)/NCG nanocomposites, respectively.

In view of the importance in practical applications, we examined thermal decomposition of the P(MMA/BMA)/NCG and P(MMA/BA)/NCG nanocomposites by thermogravimetry (TGA) under nitrogen (Figure 7). TGA and differential curves of the neat NCG, P(MMA/BMA), P(MMA/BA), and their nanocomposites containing 15% v/v NCG show improved thermal stability by the presence of NCG, suggesting that thermal decomposition of the polymer chains is suppressed by the interconnected nanofibrillar cellulose network structure of the NCG. Since these nanocomposites do not melt or decompose up to 300 °C, they can be used at much higher temperatures than neat polymers.

One problem of organic polymers in electronic application is their significant thermal expansion, which hinders accurate alignment of electronic components on the substrate involving thermal processing.[54] We further determined in-plane and out-of-plane coefficients of thermal expansion (CTEs) of the P(MMA/BMA)/NCG nanocomposites from 20 to 200 °C. Compared with the neat polymer, CTE of the nanocomposites for both directions decreased sharply by introduction of the NCG, giving in-plane CTE of 15 ppm·K^{-1} for NCG content of 78% v/v below T_g (Figure 8; see Figure S13 in the Supporting Information). Such suppression of thermal expansion is also likely to result from the presence of a rigid 3D network of cellulose. The larger thermal expansion in the thickness direction would arise from harmonic molecular oscillations and greater heat sensitivity of van der Waals interactions along this direction, suggesting a possible anisotropy in the NCG structure, with the cellulose fibrils aligning along the film surface.[22,55,56] Thus, P(MMA/BMA)/NCG and P(MMA/BA)/NCG nanocomposites are potentially useful as flexible display materials with excellent solvent resistance, high mechanical properties, moderate thermal stability, and much lower coefficients of thermal expansion.

CONCLUSIONS

In summary, the P(MMA/BMA)/NCG and P(MMA/BA)/NCG nanocomposites were fabricated via in-situ polymerization of monomers in three-dimensionally nanoporous

DOI: 10.1021/acsami.5b06232
ACS Appl. Mater. Interfaces 2015, 7, 22990–22998

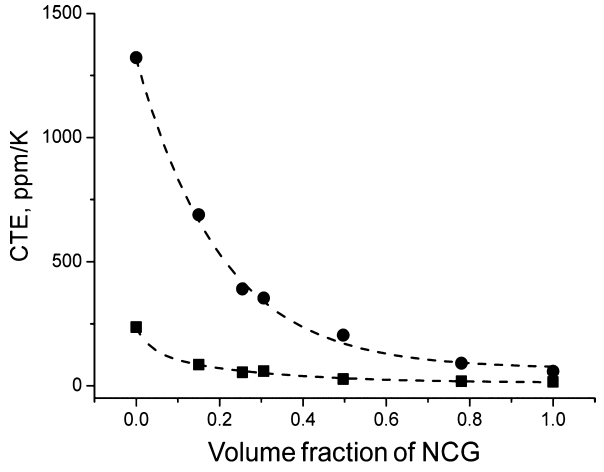

Figure 8. CTE values of the P(MMA/BMA)/NCG nanocomposites for out-of-plane (filled circle) and in-plane (filled square) coefficients as a function of volume fraction of NCG.

cellulose gel via dissolution and coagulation approaches from aqueous alkali hydroxide/urea solution. The innerconnected nanofibrillar network structure of the NCG was finely distributed and preserved well in the nanocomposites after polymerization, leading to a significant improvement in the tensile storage modulus E' above the glass transition temperature. The reinforcement effects can be explained by the percolation model. Additionally, the nanocomposites also demonstrate excellent solvent resistance, high mechanical properties, moderate thermal stability, and much lower coefficients of thermal expansion. This approach will have great promising applications in flexible display, packing, biomedical implants, and many others.

■ ASSOCIATED CONTENT

Supporting Information

The Supporting Information is available free of charge on the ACS Publications website at DOI: 10.1021/acsami.5b06232.

Photograph, SEM, AFM, XRD, FT-IR, DMA, TMA, water uptake, compression test et al. (PDF)

■ AUTHOR INFORMATION

Corresponding Author

*E-mail: caijie@whu.edu.cn. Phone: +86-27-8721-6311. Fax: +86-27-6875-4067.

Author Contributions

‡Z.S. and J.H. contributed equally to this work.

Notes

The authors declare no competing financial interest.

■ ACKNOWLEDGMENTS

This work was supported by the National Natural Science Foundation of China (21422405, 51373125) and the Major Program of National Natural Science Foundation of China (21334005). The authors are thankful to the facility support of the Natural Science Foundation of Hubei Province and the Fundamental Research Funds for the Central Universities.

■ REFERENCES

(1) Fernandes, G. E.; Kim, J. H.; Sood, A. K.; Xu, J. Giant Temperature Coefficient of Resistance in Carbon Nanotube/Phase-Change Polymer Nanocomposites. *Adv. Funct. Mater.* **2013**, *23*, 4678–4683.

(2) de Lannoy, C. F.; Jassby, D.; Gloe, K.; Gordon, A. D.; Wiesner, M. R. Aquatic Biofouling Prevention by Electrically Charged Nanocomposite Polymer Thin Film Membranes. *Environ. Sci. Technol.* **2013**, *47*, 2760–2768.

(3) Chang, C. M.; Weng, C. J.; Chien, C. M.; Chuang, T. L.; Lee, T. Y.; Yeh, J. M.; Wei, Y. Polyaniline/Carbon Nanotube Nanocomposite Electrodes with Biomimetic Hierarchical Structure for Supercapacitors. *J. Mater. Chem. A* **2013**, *1*, 14719–14728.

(4) Gu, H. B.; Tadakamalla, S.; Zhang, X.; Huang, Y. D.; Jiang, Y.; Colorado, H. A.; Luo, Z. P.; Wei, S. Y.; Guo, Z. H. Epoxy Resin Nanosuspensions and Reinforced Nanocomposites from Polyaniline Stabilized Multi-walled Carbon Nanotubes. *J. Mater. Chem. C* **2013**, *1*, 729–743.

(5) Kaiser, A. B.; Skakalova, V. Electronic Conduction in Polymers, Carbon Nanotubes and Graphene. *Chem. Soc. Rev.* **2011**, *40*, 3786–3801.

(6) Nardecchia, S.; Carriazo, D.; Ferrer, M. L.; Gutierrez, M. C.; del Monte, F. Three Dimensional Macroporous Architectures and Aerogels Built of Carbon Nanotubes and/or Graphene: Synthesis and Applications. *Chem. Soc. Rev.* **2013**, *42*, 794–830.

(7) Hu, K. S.; Gupta, M. K.; Kulkarni, D. D.; Tsukruk, V. V. Ultra-Robust Graphene Oxide-Silk Fibroin Nanocomposite Membranes. *Adv. Mater.* **2013**, *25*, 2301–2307.

(8) Cong, H. P.; Wang, P.; Yu, S. H. Stretchable and Self-healing Graphene Oxide–Polymer Composite Hydrogels: A Dual-network Design. *Chem. Mater.* **2013**, *25*, 3357–3362.

(9) Xu, K. L.; Chen, G. M.; Qiu, D. Convenient Construction of Poly(3,4-ethylenedioxythiophene)-Graphene Pie-like Structure with Enhanced Thermoelectric Performance. *J. Mater. Chem. A* **2013**, *1*, 12395–12399.

(10) Xia, L. W.; Xie, R.; Ju, X. J.; Wang, W.; Chen, Q. M.; Chu, L. Y. Nano-structured Smart Hydrogels with Rapid Response and High Elasticity. *Nat. Commun.* **2013**, *4*, 2226–2236.

(11) Ning, J. Y.; Li, G.; Haraguchi, K. Synthesis of Highly Stretchable, Mechanically Tough, Zwitterionic Sulfobetaine Nanocomposite Gels with Controlled Thermosensitivities. *Macromolecules* **2013**, *46*, 5317–5328.

(12) Tamesue, S.; Ohtani, M.; Yamada, K.; Ishida, Y.; Spruell, J. M.; Lynd, N. A.; Hawker, C. J.; Aida, T. Linear versus Dendritic Molecular Binders for Hydrogel Network Formation with Clay Nanosheets: Studies with ABA Triblock Copolyethers Carrying Guanidinium Ion Pendants. *J. Am. Chem. Soc.* **2013**, *135*, 15650–15655.

(13) Fujisawa, S.; Ikeuchi, T.; Takeuchi, M.; Saito, T.; Isogai, A. Superior Reinforcement Effect of TEMPO-Oxidized Cellulose Nanofibrils in Polystyrene Matrix: Optical, Thermal, and Mechanical Studies. *Biomacromolecules* **2012**, *13*, 2188–2194.

(14) Habibi, Y.; Lucia, L. A.; Rojas, O. J. Cellulose Nanocrystals: Chemistry, Self-Assembly, and Applications. *Chem. Rev.* **2010**, *110*, 3479–3500.

(15) Capadona, J. R.; Shanmuganathan, K.; Tyler, D. J.; Rowan, S. J.; Weder, C. Stimuli-responsive Polymer Nanocomposites Inspired by the Sea Cucumber Dermis. *Science* **2008**, *319*, 1370–1374.

(16) Capadona, J.; Van Den Berg, O.; Capadona, L.; Schroeter, M.; Rowan, S.; Tyler, D.; Weder, C. A Versatile Approach for the Processing of Polymer Nanocomposites with Self-assembled Nanofibre Templates. *Nat. Nanotechnol.* **2007**, *2*, 765–769.

(17) Dagnon, K. L.; Shanmuganathan, K.; Weder, C.; Rowan, S. J. Water-Triggered Modulus Changes of Cellulose Nanofiber Nanocomposites with Hydrophobic Polymer Matrices. *Macromolecules* **2012**, *45*, 4707–4715.

(18) Klemm, D.; Kramer, F.; Moritz, S.; Lindström, T.; Ankerfors, M.; Gray, D.; Dorris, A. Nanocelluloses: A New Family of Nature-Based Materials. *Angew. Chem., Int. Ed.* **2011**, *50*, 5438–5466.

(19) Eichhorn, S. J. Stiff as a Board: Perspectives on the Crystalline Modulus of Cellulose. *ACS Macro Lett.* **2012**, *1*, 1237–1239.

DOI: 10.1021/acsami.5b06232
ACS Appl. Mater. Interfaces 2015, 7, 22990–22998

(20) Moon, R. J.; Martini, A.; Nairn, J.; Simonsen, J.; Youngblood, J. Cellulose Nanomaterials Review: Structure, Properties and Nanocomposites. *Chem. Soc. Rev.* **2011**, *40*, 3941−3994.
(21) Quero, F.; Eichhorn, S. J.; Nogi, M.; Yano, H.; Lee, K. Y. Bismarck, A., Interfaces in Cross-Linked and Grafted Bacterial Cellulose/Poly(Lactic Acid) Resin Composites. *J. Polym. Environ.* **2012**, *20*, 916−925.
(22) Nogi, M.; Yano, H. Transparent Nanocomposites Based on Cellulose Produced by Bacteria Offer Potential Innovation in the Electronics Device Industry. *Adv. Mater.* **2008**, *20*, 1849−1852.
(23) Ifuku, S.; Nogi, M.; Abe, K.; Handa, K.; Nakatsubo, F.; Yano, H. Surface Modification of Bacterial Cellulose Nanofibers for Property Enhancement of Optically Transparent Composites: Dependence on Acetyl-group DS. *Biomacromolecules* **2007**, *8*, 1973−1978.
(24) Shopsowitz, K. E.; Qi, H.; Hamad, W. Y.; MacLachlan, M. J. Free-standing Mesoporous Silica Films with Tunable Chiral Nematic Structures. *Nature* **2010**, *468*, 422−425.
(25) Beecher, J. F. Wood, Trees and Nanotechnology. *Nat. Nanotechnol.* **2007**, *2*, 466−467.
(26) Bonini, C.; Heux, L.; Cavaille, J. Y.; Lindner, P.; Dewhurst, C.; Terech, P. Rodlike Cellulose Whiskers Coated with Surfactant: A Small-angle Neutron Scattering Characterization. *Langmuir* **2002**, *18*, 3311−3314.
(27) Habibi, Y.; Goffin, A. L.; Schiltz, N.; Duquesne, E.; Dubois, P.; Dufresne, A. Bionanocomposites Based on Poly(epsilon-caprolactone)-grafted Cellulose Nanocrystals by Ring-opening Polymerization. *J. Mater. Chem.* **2008**, *18*, 5002−5010.
(28) Ljungberg, N.; Bonini, C.; Bortolussi, F.; Boisson, C.; Heux, L.; Cavaille, J. Y. New Nanocomposite Material Reinforced with Cellulose Whiskers in Atactic Polypropylene: Effect of Surface and Dispersion Characteristics. *Biomacromolecules* **2005**, *6*, 2732−2739.
(29) Petersson, L.; Kvien, I.; Oksman, K. Structure and Thermal Properties of Poly(lactic acid)/Cellulose Whiskers Nanocomposites Materials. *Compos. Sci. Technol.* **2007**, *67*, 2535−2544.
(30) Fujisawa, S.; Saito, T.; Kimura, S.; Iwata, T.; Isogai, A. Surface Engineering of Ultrafine Cellulose Nanofibrils toward Polymer Nanocomposite Materials. *Biomacromolecules* **2013**, *14*, 1541−1546.
(31) Capadona, J. R.; Shanmuganathan, K.; Trittschuh, S.; Seidel, S.; Rowan, S. J.; Weder, C. Polymer Nanocomposites with Nanowhiskers Isolated from Microcrystalline Cellulose. *Biomacromolecules* **2009**, *10*, 712−716.
(32) Mendez, J.; Annamalai, P. K.; Eichhorn, S. J.; Rusli, R.; Rowan, S. J.; Foster, E. J.; Weder, C. Bioinspired Mechanically Adaptive Polymer Nanocomposites with Water-Activated Shape-Memory Effect. *Macromolecules* **2011**, *44*, 6827−6835.
(33) Boujemaoui, A.; Carlsson, L.; Malmström, E.; Lahcini, M.; Berglund, L.; Sehaqui, H.; Carlmark, A. Facile Preparation Route for Nanostructured Composites: Surface-Initiated Ring-Opening Polymerization of ε-Caprolactone from High-Surface-Area Nanopaper. *ACS Appl. Mater. Interfaces* **2012**, *4*, 3191−3198.
(34) Iwamoto, S.; Nakagaito, A.; Yano, H. Nano-fibrillation of Pulp Fibers for the Processing of Transparent Nanocomposites. *Appl. Phys. A: Mater. Sci. Process.* **2007**, *89*, 461−466.
(35) Suryanegara, L.; Nakagaito, A.; Yano, H. The Effect of Crystallization of PLA on the Thermal and Mechanical Properties of Microfibrillated Cellulose-reinforced PLA Composites. *Compos. Sci. Technol.* **2009**, *69*, 1187−1192.
(36) Wu, Q.; Henriksson, M.; Liu, X.; Berglund, L. A High Strength Nanocomposite Based on Microcrystalline Cellulose and Polyurethane. *Biomacromolecules* **2007**, *8*, 3687−3692.
(37) Cai, J.; Kimura, S.; Wada, M.; Kuga, S.; Zhang, L. Cellulose Aerogels from Aqueous Alkali Hydroxide-Urea Solution. *ChemSusChem* **2008**, *1*, 149−154.
(38) Cai, J.; Kimura, S.; Wada, M.; Kuga, S. Nanoporous Cellulose as Metal Nanoparticles Support. *Biomacromolecules* **2009**, *10*, 87−94.
(39) Cai, J.; Liu, S. L.; Feng, J.; Kimura, S.; Wada, M.; Kuga, S.; Zhang, L. N. Cellulose-Silica Nanocomposite Aerogels by In Situ Formation of Silica in Cellulose Gel. *Angew. Chem.* **2012**, *124*, 2118−2121.
(40) Wang, Q. Y.; Cai, J.; Zhang, L. N.; Xu, M.; Cheng, H.; Han, C. C.; Kuga, S.; Xiao, J.; Xiao, R. A Bioplastic with High Strength Constructed from a Cellulose Hydrogel by Changing the Aggregated Structure. *J. Mater. Chem. A* **2013**, *1*, 6678−6686.
(41) Cai, J.; Zhang, L. Unique Gelation Behavior of Cellulose in NaOH/Urea Aqueous Solution. *Biomacromolecules* **2006**, *7*, 183−189.
(42) Cai, J.; Liu, Y. T.; Zhang, L. N. Dilute Solution Properties of Cellulose in LiOH/Urea Aqueous System. *J. Polym. Sci., Part B: Polym. Phys.* **2006**, *44*, 3093−3101.
(43) Cai, J.; Zhang, L. Rapid Dissolution of Cellulose in LiOH/Urea and NaOH/Urea Aqueous Solutions. *Macromol. Biosci.* **2005**, *5*, 539−548.
(44) Siqueira, G.; Bras, J.; Dufresne, A. Cellulose Whiskers versus Microfibrils: Influence of the Nature of the Nanoparticle and its Surface Functionalization on the Thermal and Mechanical Properties of Nanocomposites. *Biomacromolecules* **2009**, *10*, 425−432.
(45) Ouali, N.; Cavaille, J. Y.; Perez, J. Elastic, viscoelastic and plastic behavior of multiphase polymer blends. *Plast., Rubber Compos. Process. Appl.* **1991**, *16*, 55−60.
(46) Favier, V.; Cavaille, J. Y.; Canova, G. R.; Shrivastava, S. C. Mechanical Percolation in Cellulose Whisker Nanocomposites. *Polym. Eng. Sci.* **1997**, *37*, 1732−1739.
(47) Dubief, D.; Samain, E.; Dufresne, A. Polysaccharide Microcrystals Reinforced Amorphous Poly(β-hydroxyoctanoate) Nanocomposite Materials. *Macromolecules* **1999**, *32*, 5765−5771.
(48) Tang, L.; Weder, C. Cellulose Whisker/Epoxy Resin Nanocomposites. *ACS Appl. Mater. Interfaces* **2010**, *2*, 1073−1080.
(49) Jorfi, M.; Roberts, M. N.; Foster, E. J.; Weder, C. Physiologically Responsive, Mechanically Adaptive Bio-Nanocomposites for Biomedical Applications. *ACS Appl. Mater. Interfaces* **2013**, *5*, 1517−1526.
(50) Roohani, M.; Habibi, Y.; Belgacem, N. M.; Ebrahim, G.; Karimi, A. N.; Dufresne, A. Cellulose Whiskers Reinforced Polyvinyl Alcohol Copolymers Nanocomposites. *Eur. Polym. J.* **2008**, *44*, 2489−2498.
(51) Braun, B.; Dorgan, J. R.; Hollingsworth, L. O. Supra-Molecular EcoBioNanocomposites Based on Polylactide and Cellulosic Nanowhiskers: Synthesis and Properties. *Biomacromolecules* **2012**, *13*, 2013−2019.
(52) Alloin, F.; D'Aprea, A.; Kissi, N. E.; Dufresne, A.; Bossard, F. Nanocomposite Polymer Electrolyte Based on Whisker or Microfibrils Polyoxyethylene Nanocomposites. *Electrochim. Acta* **2010**, *55*, 5186−5194.
(53) Dufresne, A.; Cavaillé, J.-Y.; Helbert, W. Thermoplastic Nanocomposites Filled with Wheat Straw Cellulose Whiskers. Part II: Effect of Processing and Modeling. *Polym. Compos.* **1997**, *18*, 198−210.
(54) MacDonald, W. A. Engineered Films for Display Technologies. *J. Mater. Chem.* **2004**, *14*, 4−10.
(55) Langan, P.; Sukumar, N.; Nishiyama, Y.; Chanzy, H. Synchrotron X-ray Structures of Cellulose Iβ and Regenerated Cellulose II at Ambient Temperature and 100 K. *Cellulose* **2005**, *12*, 551−562.
(56) Hori, R.; Wada, M. The Thermal Expansion of Cellulose II and III_{II} Crystals. *Cellulose* **2006**, *13*, 281−290.

DOI: 10.1021/acsami.5b06232
ACS Appl. Mater. Interfaces 2015, 7, 22990−22998